This is an open access article published under a Creative Commons Attribution (CC-BY) License, which permits unrestricted use, distribution and reproduction in any medium, provided the author and source are cited.

ACS AUTHORCHOICE

CHEMISTRY OF MATERIALS

pubs.acs.org/cm Article

Area-Selective Molecular Layer Deposition of Polyimide on Cu through Cu-Catalyzed Formation of a Crystalline Interchain Polyimide

Chao Zhang, Marko Vehkamäki, Mika Pietikäinen, Markku Leskelä, and Mikko Ritala*

Cite This: *Chem. Mater.* 2020, 32, 5073−5083 Read Online

ACCESS | Metrics & More | Article Recommendations | Supporting Information

Downloaded via UNIV OF HELSINKI on September 24, 2020 at 10:49:41 (UTC).
See https://pubs.acs.org/sharingguidelines for options on how to legitimately share published articles.

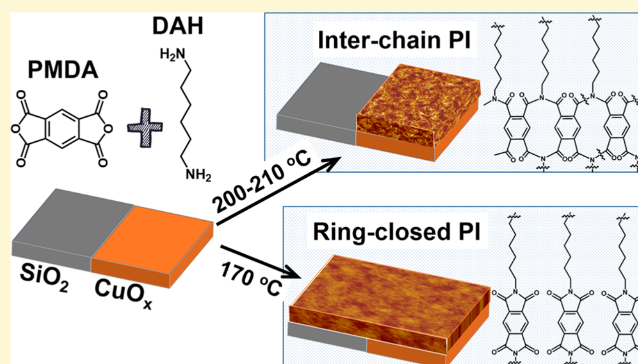

ABSTRACT: Novel area-selective molecular layer deposition (AS-MLD) of polyimide (PI) on Cu versus native SiO_2 was studied. By use of 1,6-diaminohexane (DAH) and pyromellitic dianhydride (PMDA) as precursors, PI films can be selectively deposited on the Cu surface at 200−210 °C with a rate around 7.8 Å/cycle while negligible growth takes place on SiO_2. The selectivity was successfully demonstrated also on Cu/SiO_2 patterns at 200 °C; after 180 MLD cycles, around 140 nm thick PI was deposited on Cu regions while <10 nm thick PI was measured on SiO_2 regions. By contrast, at 170 °C, similar growth rates were measured on Cu (4 Å/cycle) and native SiO_2 (5 Å/cycle). To understand the origin of the selectivity, properties of PI film grown on Cu at the selectivity enabling temperature of 200 °C have been thoroughly compared with those grown on both Cu and native SiO_2 at the nonselective temperature of 170 °C. Significant differences in crystallinity, surface morphology, and chemical structure suggest that the PI films grown on Cu at 200 °C have a novel crystalline interchain PI structure. According to this finding, the selectivity mechanism is proposed to derive from a new MLD reaction mechanism catalyzed by copper ions at 200−210 °C that leads to the formation of new crystalline polymer species. Additionally, it is suggested that small amounts of Cu ions can float on the surface of the growing PI film and thereby constantly catalyze the MLD reaction, as evidenced by XRD, XPS, and ToF-ERDA. The high catalytic efficiency has been also proven by using successfully an ultrathin Cu layer, nominally 0.1 nm, as a seed layer to initiate the MLD growth.

1. INTRODUCTION

As the feature sizes in nanoelectronics keep scaling downward, conventional photolithography that has served as a long-term reliable approach for semiconductor nanofabrication is facing greater challenges than ever in terms of resolution, edge placement accuracy, and cost-efficiency.[1,2] Area-selective deposition (ASD) as an alternative scheme has therefore been gaining a lot of interest lately.[3] In contrast to the top-down lithography based on etching, nanopatterning by ASD is a bottom-up approach to selectively deposit film material only at the desired surface regions without the need for etching. Moreover, the capability to direct the film deposition in a fully self-aligned manner offers ASD great potential as a more efficient and reliable nanopatterning technique to complement or even replace the current lithography route.[4]

In the family of ASD techniques, area-selective atomic layer deposition (AS-ALD) has been extensively studied due to both the unique properties of ALD[5] and the feasibility to control ALD growth spatially by simply modifying chemical nature of the substrate surface.[6] It is well-known that the ALD growth is initiated by surface reactions between vapor-phase precursors and reactive sites present on the substrate surface. Therefore, by locally manipulating the surface chemistry of the substrate before ALD, we can limit the film growth to specific regions while the other parts of the surface keep intact. AS-ALD by surface modification can be classified into two main categories: surface passivation and surface activation. AS-ALD by surface passivation means that selected parts of substrate surfaces are tailored inert toward the ALD chemistry. Self-assembled monolayers (SAMs) with $-CH_3$ tail groups are commonly employed as surface modifiers to convert the substrate surface inert and thus prevent the subsequent ALD growth.[7−10] Alternatively, instead of deactivating the substrate surface, AS-ALD can be achieved by locally promoting the ALD growth on an otherwise inert substrate surface with the use of a prepatterned seed layer as a growth stimulator. This seed layer can either catalyze the ALD reaction[11−14] or provide

Received: March 2, 2020
Revised: June 3, 2020
Published: June 3, 2020

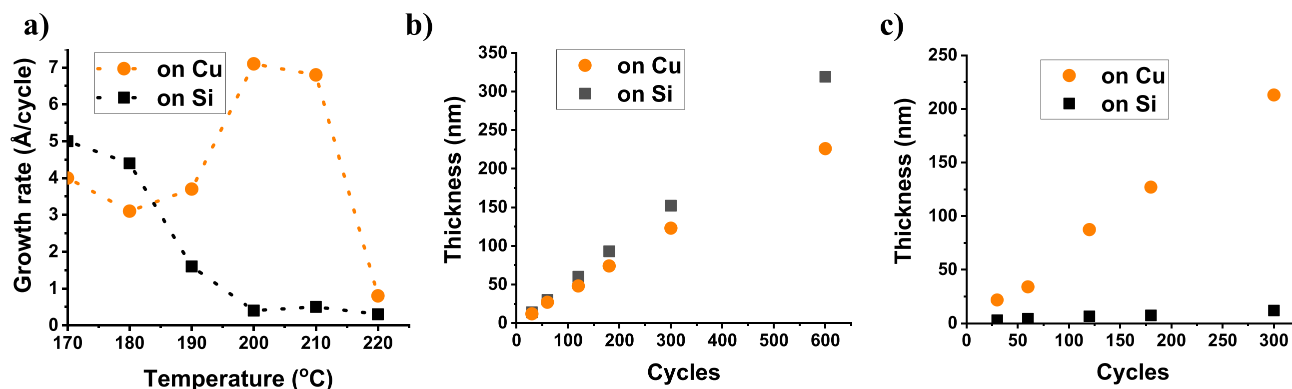

Figure 1. (a) Growth rate of PI MLD on Cu and native SiO_2 as a function of deposition temperature. (b, c) PI thickness as a function of the number of MLD cycles; the PI films were deposited on both native SiO_2 and Cu at (b) 170 °C and (c) 200 °C. Pulse and purge time for the DAH precursor were kept at 2 and 3 s, respectively, while for PMDA 5 s was used for both pulse and purge. Film thicknesses were measured by ellipsometry.

reactive sites to initiate the ALD growth.[15,16] This strategy can be extended to a fully self-aligned approach in which ALD films selectively grow on certain materials exposed on the surface because of the underlying device structures. Consequently, film patterning can be done in only one step, which simplifies the patterning process greatly. The self-aligned process also provides a solution to the edge placement error (EPE) in multilayer structure patterning.

Because of the great potential in semiconductor processing and catalysis,[17,18] AS-ALD that bases on the growth activation through a catalytic effect of the underlying substrate has been studied and reported in some papers. The previous work in our group by Färm et al. showed that microcontact printed RuO_x seed layers efficiently activate the Ru ALD process when $RuCp_2$ and O_2 were used as precursors at a deposition temperature of 250 °C so that the Ru film was deposited only on the seed layer patterns but not on bare SiO_2.[14] By using electron beam or ion-beam induced deposition (EBID or IBID) to write patterns of a thin noble metal seed layer before the ALD processes, AS-ALD of Pt[12,13] and metal oxides (iron oxide and nickel oxide)[11] has been achieved by Mackus et al. Herein, we extend this approach to selective deposition of an organic polymer by MLD using the catalytic effect of Cu. As an extension of ALD, MLD is an enabling technique for depositing high-quality nanoscale coatings of organic polymers[19−22] and organic−inorganic hybrid materials.[23,24] Similarly to ALD, MLD is a surface-controlled gas-phase process in which molecular fragments are precisely assembled on the substrate surface in a self-limiting layer-by-layer mode.[25] MLD has shown great potential for applications such as microelectronics,[26] catalysis,[27] batteries,[28] solar cells, and many others.[29,30] Because of the need for patterned organic thin films on devices, significant efforts have been made to develop simple yet efficient strategies for patterning organic thin films.[27,31−34] Among them, AS-MLD is regarded as a superior tool due to the same advantages as AS-ALD.[35−37]

In this work, a novel approach for area-selective deposition of polyimide (PI) on Cu by MLD is studied. This is the first AS-MLD process that exploits the catalytic effect of the underlying substrate surface to achieve the selective growth of organic polymers. Earlier, surface modifiers, SAMs, have been used to prevent MLD growth.[36,37] PIs are a class of high-performance polymers with a broad range of applications due to their outstanding properties such as exceptional mechanical strength, excellent resistance to heat, chemicals, and radiation, and good dielectric properties. For instance, the semiconductor industry has considered PI thin films to be potential low-*k* dielectrics,[38−40] and gate dielectrics in organic thin-film transistors.[41−43]

The present work deals with several aspects of this novel AS-MLD approach. First, the conditions for selective deposition were identified concerning the deposition temperature and the thickness of the Cu seed layer. To determine the deposition temperature range for optimal selectivity, we examined the effect of the growth temperature on the selectivity by comparing the PI growth rate on Cu and native SiO_2. Furthermore, for the potential use of a thin Cu film as a catalytic seed layer to promote PI growth on any inert surface, it is essential to determine the effect of the thickness of the Cu seed layer on the selective PI growth. For this study, Cu seed layers with thicknesses varying from 0.1 to 150 nm were tested. Next, the selective growth of PI on patterned Cu/SiO_2 surfaces was successfully demonstrated at 200 °C by SEM and EDS. Finally, properties of PI films deposited on Cu at the selectivity enabling temperature of 200 °C were compared with those deposited on both Cu and native SiO_2 at the nonselective temperature of 170 °C. Significant differences in crystallinity, surface morphology, and chemical structure were identified by XRD, AFM, and ATR-FTIR, respectively. The differences in film properties suggest that a new type of crystalline PI is formed on Cu at 200 °C. Based on our experimental evidence and a well-known imidization mechanism of PI formation, a mechanism for the selective formation of the polymer with a novel structure on Cu by MLD is proposed.

2. EXPERIMENTAL SECTION

2.1. Film Deposition. PI thin films were deposited in a hot-wall, cross-flow F120 ALD reactor (ASM Microchemistry) with an operating pressure of around 10 mbar. Nitrogen (N_2, AGA, 99.999%) was used as the carrier and purge gas. Pyromellitic dianhydride (PMDA) and 1,6-diaminohexane (DAH), purchased from Sigma-Aldrich, were evaporated inside the reactor at 45 and 165 °C, respectively. The pulse and purge times for DAH were 2 and 3 s, respectively. For PMDA, they were both 5 s. Films were deposited on 5 × 5 cm^2 native SiO_2-terminated and Cu-coated Si substrates at temperatures of 170−220 °C with different numbers of MLD cycles. The Si substrates were p-type Si (100) with ∼1.5 nm native oxide on top. Cu-coated Si substrates had different Cu thicknesses of 0.1, 1.0, 2.5, 5, 10, and 150 nm. The Cu layers with thicknesses of 10 nm and below were prepared by electron beam evaporation directly on Si, and

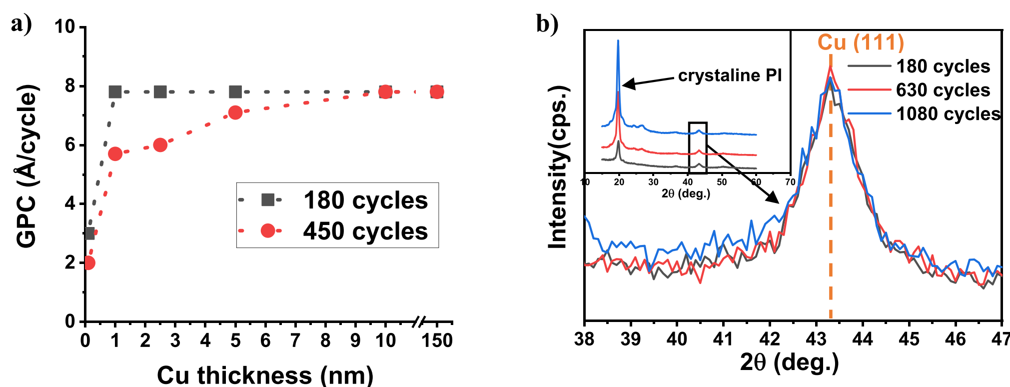

Figure 2. (a) Growth rate of PI MLD at 200 °C on Cu seed layers with different thicknesses from 0.1 to 150 nm at the number of MLD cycles of 180 and 450 cycles. The PI film thicknesses were measured by cross-sectional SEM (b) Intensity of the Cu (111) diffraction peak measured from 5 nm thick Cu layer after PI deposition with 180, 630, and 1080 MLD cycles. Inset: the intensity of the diffraction peak from the crystalline PI film (to be discussed in section 3.3.1).

their thicknesses were measured by quartz crystal microbalance (QCM) during the evaporation. The 150 nm Cu-coated Si wafers were received from ASMM. These Cu layers had an adhesion layer of around 15 nm Ta underneath. Unless otherwise noted, the Cu films were used as received without any chemical pretreatment, meaning that a layer of CuO_x, formed upon air exposure, was present on the surfaces.

2.2. Preparation of Patterned Cu/Native SiO_2 Samples. Patterned Cu/SiO_2 samples were prepared by evaporating an ~15 nm thick Cu film on Si wafer through a shadow mask. The resulting patterns had ~50 μm wide Cu lines and ~50 μm native SiO_2 spacers in between. Selective deposition of PI on this patterned Cu/SiO_2 surface was tested at 200 °C with 180 MLD cycles.

2.3. Film Characterization. Thicknesses of PI films were measured by a FS-1 multiwavelength ellipsometer (Film Sense) and cross-sectional SEM (Hitachi S-4800). Surface morphology was determined by atomic force microscopy (AFM, Veeco Multimode V instrument). The measurements were performed in air by using Si probes with a tip radius of 10 nm and a spring constant of 5 N/m (Tap150 from Bruker). The images were flattened, and the roughness was calculated as a root-mean-square value (R_q). The crystallinity of the films was measured by a Rigaku Smartlab diffractometer using Cu Kα radiation with an incident angle of 1°. Bonding information about the as-deposited PI films was obtained from attenuated total reflection Fourier transform infrared (ATR-FTIR) spectra. We characterized the surface composition of PI films by X-ray photoelectron spectroscopy (XPS) using a K-alpha X-ray photoelectron spectrometer (XPS) system (ThermoFisher) operating at a pass energy of 200 eV for survey scans and 30 eV for high-resolution scans. Samples were illuminated with X-rays emitted from an Al source (Kα line) at a photon energy of 1486.7 eV. The success in depositing PI selectively on Cu regions versus native SiO_2 regions was demonstrated by SEM and EDX using a Hitachi S-4800 field emission scanning electron microscope equipped with an INCA 350 EDX spectrometer.

3. RESULTS AND DISCUSSION

3.1. Selective Growth Conditions. *3.1.1. Selective Growth of PI on Cu versus Native SiO_2: Effect of Deposition Temperature.* Figure 1a shows a comparison of growth rates of PI films on 150 nm Cu-coated Si and SiO_2-terminated Si substrates at deposition temperatures of 170−220 °C. The lower limit for the deposition temperature was 170 °C to avoid precursor condensation because the evaporation temperature of PMDA was 165 °C. The upper limit was 220 °C where the growth rates on both substrates approach zero. Within the examined temperature range, the PI growth rates on both Cu and native SiO_2 depend largely but differently on the deposition temperature. On the native SiO_2, the PI growth rate decreases steadily with increasing temperature, from 5 Å/cycle at 170 °C to almost zero at 200−220 °C, as reported earlier.[20] By contrast, on Cu an increase was observed in the temperature range of 180−200 °C. Notably, this increase was suddenly accelerated at 200 °C, where the selective growth of PI on Cu was significant. Only at 220 °C was the growth rate on Cu close to zero. It is common for MLD processes that growth rates decrease with increasing temperature[20,24,25,44,45] due to either the desorption of MLD precursors[46] or the consumption of both reactive ends of organic precursor molecules by "double reactions".[24] The unusual increase in the PI MLD rate on Cu at 180−200 °C is assumed to arise from a new MLD reaction which becomes possible at higher temperatures. This new MLD reaction was proved by the finding of new polymer species in the deposited PI films, as evidenced by XRD, AFM, and ATR-FTIR results presented in section 3.3.

The relationship between the PI film thickness and the number of MLD cycles was investigated on Cu and native SiO_2 at both 170 and 200 °C where 170 °C represents the nonselective temperature region and 200 °C the selectivity enabling temperature region. At 170 °C the growth rates on Cu and native SiO_2 are 5 and 4 Å/cycle, respectively. On both substrates, the growth is linear within the studied 600 MLD cycles (Figure 1b). On the other hand, at 200 °C a remarkable selective growth of PI on Cu versus native SiO_2 was observed (Figure 1c). The thickness difference of PI on these two surfaces gets more pronounced as the number of MLD cycles increases. Even after 300 MLD cycles the PI thickness on native SiO_2 is still much lower than that on Cu: <10 nm PI was deposited on native SiO_2 while ~230 nm PI was grown on Cu. Such a large thickness difference suggests that the main cause for the slow growth on native SiO_2 lays in unfavorable surface reactions between the two precursors, DAH and PMDA, during the steady-state film growth, rather than in a difficulty of film nucleation on native SiO_2. This is different from AS-ALD that relies on differences in nucleation delays on growth and nongrowth regions and the selectivity often lasts for only tens of ALD cycles, corresponding to a selective deposition of a few nm films on the growth surfaces.[16,47−51] Such a limited selectivity is caused by the fact that the nucleation of ALD films eventually takes place also on the nongrowth surfaces. Once the nongrowth surfaces are fully covered with the nuclei, subsequent undifferentiated growth occurs on the growth and

https://dx.doi.org/10.1021/acs.chemmater.0c00898
Chem. Mater. 2020, 32, 5073−5083

nongrowth regions. Therefore, the comparatively much lower growth rate of PI on native SiO_2 even after 300 MLD cycles also suggests that the selective growth is most likely caused by a different MLD reaction which preferably proceeds on Cu rather than on native SiO_2 at 200−210 °C. Because of the 10 nm PI deposited on native SiO_2, a time-controlled etchback with, for example, oxygen plasma would be needed for the completely selective outcome. Such etchbacks have become increasingly adopted for correcting area selective deposition processes through a removal of minor deposits from nongrowth surfaces.[52−54]

3.1.2. Selective MLD Growth on Cu Seed Layers with Various Thicknesses. A study of the influence of the Cu seed layer thickness on the selective MLD growth is important for applications where it is essential to use as thin a Cu layer as possible as an activator to promote the PI growth on regions of interest. Also, this study provides convincing evidence to our hypothesis of Cu-catalyzed MLD reaction in a continuous mode through Cu ions floating on the surface of the growing PI film (section 3.3).

Cu films with different thicknesses (0.1, 1.0, 2.5, 5, 10, and 150 nm) were studied as seed layers. PI growth on these Cu layers was investigated at 200 °C with 180 and 450 MLD cycles. The plots of PI growth rates versus the Cu thickness are shown in Figure 2a. The PI film thicknesses were measured from cross-sectional SEM images. Although the PI growth rate is somewhat dependent on the Cu thickness, the variations are small. For 180 MLD cycles, already 1 nm Cu layer is sufficiently thick to achieve the maximum growth rate of ∼7.8 Å/cycle. On the other hand, for 450 MLD cycles 10 nm Cu seed layer is needed for the full growth rate, though only a slightly lower growth rate of 6 Å/cycle was measured on 1 nm Cu layer. We also studied the MLD growth on an ultrathin Cu seed layer with a nominal thickness of only 0.1 nm. Interestingly, PI can grow on this ultrathin Cu layer but with a lower growth rate of 3 Å/cycle for 180 MLD cycles and 2 Å/cycle for 450 MLD cycles. The catalytic efficiency of Cu ions is thus high as trace amounts of Cu are enough to initiate and support the film growth. Although a thicker Cu layer is needed to attain the maximum growth rate for a higher number of MLD cycles, the differences in growth rates are small. This result proves, indirectly, that Cu ions float on the surface of the growing PI film, constantly and efficiently catalyzing the MLD reaction. Thereby, only small amounts of Cu are needed for continuous film growth. This also implies that the Cu layer is not extensively consumed during the PI growth. Indeed, we demonstrated that a PI film with a thickness of ∼800 nm, corresponding to 1080 MLD cycles, can be deposited on a 5 nm thick Cu layer without a detectable consumption of the Cu seed layer, as characterized by XRD (Figure 2b).

3.1.3. PI MLD on Reduced Copper Surfaces. The importance of surface oxide CuO_x (x = 1−2) on the Cu seed layer as a source of Cu ions for the selective MLD process was demonstrated by pulsing formic acid into the reaction chamber right before the PI MLD process at 200 °C. Formic acid is known to reduce the surface CuO_x to metallic Cu.[55,56] After 300 MLD cycles, only 20 nm thick PI was measured on the reduced substrate whereas more than 200 nm PI was deposited on a nonreduced copper surface. This result proves that it is most likely copper ions from the surface CuO_x that catalyze the PI growth and thereby enable the selective growth on copper.

3.2. Selectivity Demonstration on Patterns of Cu and Native SiO_2. Selective deposition of PI on Cu versus native SiO_2 was successfully demonstrated on patterned Cu/native SiO_2 surfaces with feature sizes in the micrometer scale. The deposition temperature was selected at 200 °C where optimal selectivity was observed. After 180 MLD cycles, top-view and cross-sectional SEM images clearly show that PI was selectively grown on the Cu region (the top row of images in Figure 3).

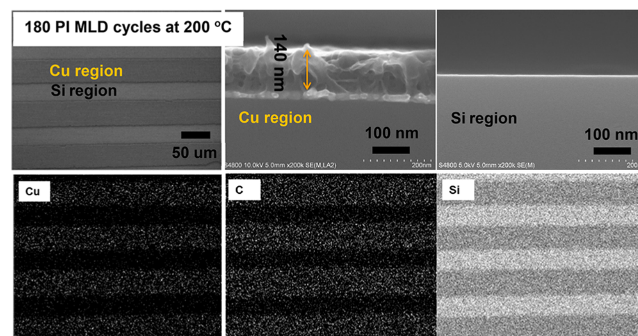

Figure 3. Patterned Cu/native SiO_2 surfaces after 180 PI MLD cycles: top-view and cross-sectional SEM images (top row); EDX images to show the distribution of Cu, Si, and C elements (bottom row).

There is around 140 nm PI grown on the Cu region while negligible PI was deposited on the Si region (there should be around 10 nm PI on native SiO_2, which is too thin to be visible in cross-sectional SEM because of charging, beam damage, and the edge contrast). The bottom row in Figure 3 shows energy dispersive X-ray maps of the Cu, C, and Si distributions on this sample. The strong C signal on the Cu region indicates that PI films were selectively deposited on Cu, consistent with the observations from the cross-sectional SEM images.

3.3. Film Characterization. To the best of the authors' knowledge, this is the first time MLD growth of PI on Cu was conducted. Significant selective growth of PI on Cu versus native SiO_2 at 200−210 °C suggests that a new MLD reaction could take place on Cu at these temperatures. Fundamental understanding of reaction mechanisms in polymer MLD on a substrate surface that possesses a catalytic effect would be valuable for the design of new AS-MLD chemistries. Furthermore, as will be shown below, in our study a new crystalline interchain PI was synthesized and identified, which can bring up new applications for the MLD−PI system.[57]

The key to the understanding of the reaction mechanism in the PI MLD on Cu is to characterize the polymer species actually formed in the film. In many of the previous studies,[20,44,58−62] ring-closed PI (Figure 4) is implicitly assumed as the main product after polycondensation reactions regardless of the film preparation method. However, it has been noted that other species can also form as byproducts.

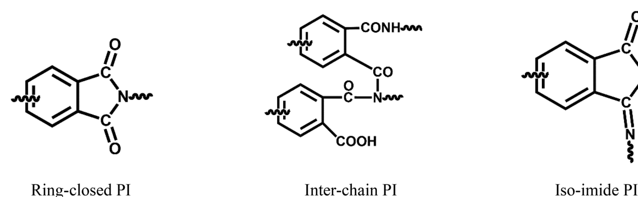

Figure 4. Possible polymer species formed in polycondensation reactions between dianhydride and diamine.

https://dx.doi.org/10.1021/acs.chemmater.0c00898
Chem. Mater. 2020, 32, 5073−5083

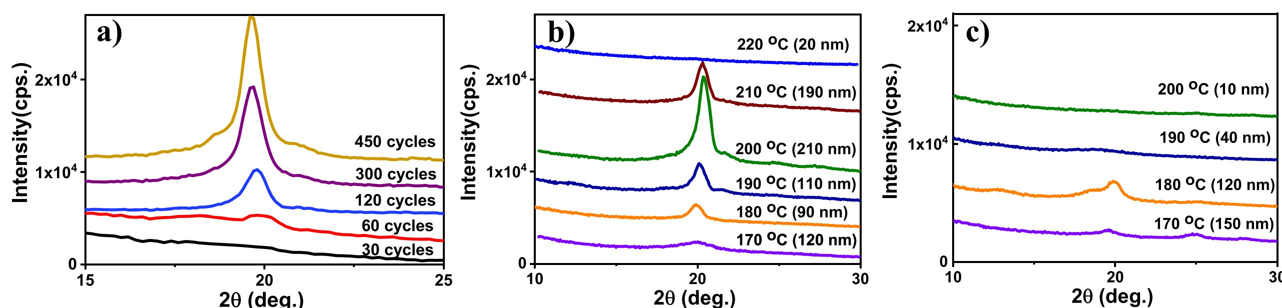

Figure 5. XRD patterns of polyimide deposited on Cu (a) at 200 °C with different MLD counts and (b) at different deposition temperatures with 300 MLD cycles. (c) XRD patterns of PI deposited on native SiO_2 at different deposition temperatures.

Commonly proposed byproducts are interchain and isoimide PIs, as shown in Figure 4.[63−65] The relative proportions of these byproducts are generally at a low level, depending on the reaction conditions and the types of monomer precursors being used. As compared with the isoimide, the interchain PI with a distinct 3D network structure has been more frequently reported. Although IR spectroscopy has been widely utilized to identify polymer species in the previous studies, it is extremely challenging to distinguish these similar polymer species from each other by only IR spectra because of the overlap of the characteristic IR bands in the PI systems.[60,66] Therefore, in this work XRD, AFM, and ATR-FTIR were used together to thoroughly investigate film properties in terms of crystallinity, surface morphology, and chemical structure.

3.3.1. Film Crystallinity: XRD. As mentioned in the literature, crystallinity of PI films can arise from both rigid molecular structures of monomer precursors[65,67] and intermolecular bonding between adjacent polymer chains forming a 3D network structure.[65,68] In our study, although the dianhydride precursor PMDA exhibits a rigid molecular structure, the coreactant DAH has a flexible long carbon-chain structure. This flexibility in the polymer chain prevents the ring-closed PI from crystallizing. The previous study[20] on PI MLD on native SiO_2 at 160−200 °C by Putkonen et al. confirmed that the as-deposited PI films were amorphous and the films also remained amorphous after postannealing at 200−400 °C. As already mentioned, besides the amorphous ring-closed PI, two possible byproducts can form during imidization: the interchain and isoimide PIs. Regardless of the monomer combination used, the interchain PI exclusively presents a high degree of crystallinity, arising from its unique network structure. Thus, by XRD measurements the identification of the interchain PI becomes facile.

In this work, XRD has been used to identify the formation of the crystalline interchain PI according to the diffraction peak at $2\theta = 20°$, attributed to intermolecular ordering as suggested in many previous studies.[67,69−71] In addition, by monitoring the peak intensity as a function of the deposition temperature, one can study the effect of the deposition temperature on the formation of the interchain PI during the MLD process. This understanding provides additional insights into the selectivity mechanism of the PI MLD process since the selectivity is heavily temperature dependent.

Figure 5a shows XRD patterns of PI films deposited on Cu at 200 °C with different cycle numbers, corresponding to different film thicknesses. The observation of a clear diffraction peak at $2\theta = 20°$ at 120 MLD cycles and above indicates the formation of the interchain PI in the deposited film. The peak intensity increases constantly with the MLD cycles. This increase can be caused by enhanced film crystallinity of the interchain PI in the deposited film or more simply by the increase of film thickness with a larger number of MLD cycles. The effect of postannealing of ∼200 nm thick PI film deposited on Cu at 200 °C was also studied. After the annealing at 200 °C for 1−6 h, the PI films were characterized by XRD immediately. No obvious changes in both peak intensity and shape were observed as compared to the unannealed sample, suggesting that at 200 °C the film crystallinity does not vary with the annealing time. Therefore, it is concluded that rather than increased film crystallinity, the formation of a thicker film, i.e., the higher volume of the interchain PI, is the reason for the constant increase in the peak intensity as the number of MLD cycles increases.

Figure 5b depicts the effect of the deposition temperature on the intensity of the diffraction peak. These films were deposited on Cu surfaces at temperatures of 170−220 °C with 300 MLD cycles. A clear crystalline peak appears at 180 °C, suggesting that the interchain PI starts to form already at such a low temperature though with only a small proportion present in the film; i.e., the formation of the amorphous ring-closed PI still dominates at 180 °C. A slow increase in the peak intensity is observed within the temperature range 170−190 °C, whereas a sharp increase occurs at 200 °C. At this temperature also a rapid increase in the film growth rate was measured (Figure 1a). Specifically, the growth rate at 200 °C is around 7.8 Å/cycle, which is 2 times higher than that at 190 °C. The simultaneous rapid increase in both the growth rate and the intensity of crystallinity suggests that 200 °C, found as the optimal temperature for the selectivity, is the transition temperature where the interchain PI starts to form substantially and the interchain PI is most likely the main product in the polymer film deposited on Cu. Above 200 °C, the peak intensity drastically decreases to zero at 220 °C, corresponding to the sharp decrease in the growth rate, i.e., film thickness. The decrease in the growth rate on Cu is similar to that on native SiO_2, suggesting precursor desorption to occur also in the PI MLD on Cu, but at higher temperatures than on SiO_2.

Interchain PI was also observed on native SiO_2 at 180 °C, as seen in Figure 5c. Although this peak is quite weak, it is still comparable to the peak measured on Cu at the same deposition temperature (Figure 5b). The result is well in line with the previous reports[63−65] that byproducts, especially interchain PI, form during thermal imidization processes. This diffraction peak, however, disappears at temperatures above 180 °C, which is understandable since much thinner PI films were deposited on SiO_2 at these temperatures.

https://dx.doi.org/10.1021/acs.chemmater.0c00898
Chem. Mater. 2020, 32, 5073−5083

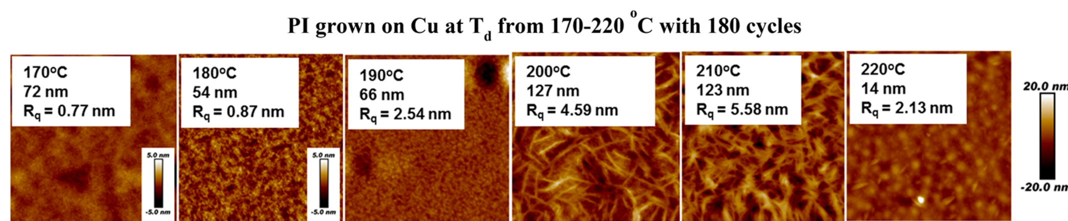

Figure 6. AFM images of PI films grown on Cu with 180 MLD cycles at different deposition temperatures. The labels show the film roughnesses (R_q) and thicknesses.

3.3.2. Surface Morphology: AFM. The morphology of PI films was characterized by AFM. Figure 6 shows the morphology evolution of PI films grown with 180 cycles on Cu with the deposition temperature increasing from 170 to 220 °C. Figure S1 presents a more comprehensive AFM study of the evolution of PI films on both Cu and native SiO_2 at 170 and 200 °C with the number of MLD cycles.

As seen in Figure S1, the films grown at 170 °C on both Cu and native SiO_2 are smooth and featureless, as characteristic of amorphous ring-closed PI thin films. This agrees well with the XRD measurements. Surface roughnesses of all these PI films are around 0.3−0.7 nm with only one exception, which is the thinnest PI film grown on Cu with 30 cycles. The higher surface roughness of 2.7 nm for this sample is caused by the roughness of the pristine Cu surface (2.6 nm). As the number of MLD cycles increases, the surface gets smoother because the amorphous PI film planarizes the original surface.

When the PI MLD is performed at 200 °C, the PI growth rate on native SiO_2 is only 0.4 Å/cycle. Although the surface roughness of the deposited film increases rapidly with MLD cycles from 2.8 nm at 30 cycles to 11.9 nm at 300 cycles, no obvious crystalline morphology is detected. Interestingly, on the Cu surface the film deposited with only 30 cycles shows fiberlike features. These features get more pronounced as the number of MLD cycles increases. At 300 MLD cycles, however, the fiberlike features are somehow suppressed. It is suggested that CVD-like growth could take place inside the film due to the obvious porosity observed on the film surface. The monomers can get trapped inside the pores and react there when the other monomer is supplied. Another possible reason is that the fragile polymer structure cannot support the increased inner stress as the film is getting thicker. At a certain thickness, the fiberlike structure starts to collapse, resulting in a partial disappearance of the features. To the best of the authors' knowledge, this is the first time when these fiberlike features were observed on PI films, supporting the formation of a new kind of crystalline polymer on the Cu surface at 200 °C. On the basis of the previous studies on PI, as discussed above, the interchain PI appears as the only possible candidate for the new polymer species.

Figure 6 depicts the effect of the deposition temperature on the surface morphology of PI films deposited on Cu. Within the studied deposition temperatures of 170−220 °C, the fiberlike features can be observed only at 200 and 210 °C. This observation is consistent with the XRD measurements where the PI film grown at 200 °C showed the most intense diffraction peak. The fiberlike features seen in the AFM image of the 127 nm thick PI film, grown on 150 nm Cu with 180 MLD cycles at 200 °C, have an average width of around 40 nm and an average length of nearly 350 nm. These dimensions are much larger than the crystallite size of 6 nm estimated from the XRD peak broadening by using the Scherrer equation, indicating that the features cannot be single crystals but grains formed from several crystals.

3.3.3. Chemical Structure: ATR-FTIR. ATR-FTIR is a sensitive characterization method for identifying organic groups in polymer films by monitoring vibrations of atoms and molecules. Assignments for the major peaks between 700 and 1980 cm^{-1} in different ring-closed polyimides are listed in Table 1. As discussed previously, both interchain PI and ring-closed PI can form during the PI MLD process. In the case of the PMDA−DAH PI, the formation of the ring-closed PI is often followed by monitoring the continuous increase of the peaks at 1772, 1712, 1380, and 728 cm^{-1}. Although the interchain PI has been frequently reported, no clear characteristic IR bands for the interchain PI have been reported yet. Some papers, however, suggest that the formation of the interchain polyimide can be monitored by following the asymmetrical C═O stretch (for PMDA−DAH around 1712 cm^{-1}) coming from both the interchain and ring-closed PI against the characteristic IR band at 1380 cm^{-1} that comes only from the ring-closed PI.[64,65]

Table 1. Peak Assignments for Different Ring-Closed PIs

	imide sym C═O	imide asym C═O stretch	imide C−N stretch	imide ring deformation or carbonyl group
PMDA−ODA[60]	1775	1724	1378	weak
PMDA−PDA[61]	1776	1721	1363	818
BTDA−ODA[72]	1780	1726	1375	719
BPDA−PDA[72]	1776	1719	1359	742
PMDA−DAH[20]	1772	1712	1380	728

Figure 7 shows the ATR-FTIR spectra of PI films deposited on native SiO_2 and Cu at 170 and 200 °C. For the PI films grown at 170 °C, all the characteristic IR bands (1772, 1712, 1380, and 728 cm^{-1}) increase with increasing MLD cycle numbers, indicating the continuous formation of the ring-closed polyimide on both SiO_2 and Cu surfaces. In the meantime, for the PI films grown on Cu at 200 °C the 1712 cm^{-1} IR band increases drastically while no noticeable increase is observed for the 1380 cm^{-1} IR band. This indicates the predominant formation of the interchain PI. The observations from IR agree well with the XRD and AFM results.

3.3.4. Surface Composition: XPS. High-resolution XPS was performed on different PI samples where the PI films were deposited on Cu (a) with the same number of MLD cycle (450 cycles) but with a different Cu thickness from 0.1 to 100 nm and (b) with the same Cu thickness (5 nm) but with a different number of MLD cycles from 450 to 1350 (Figure 8).

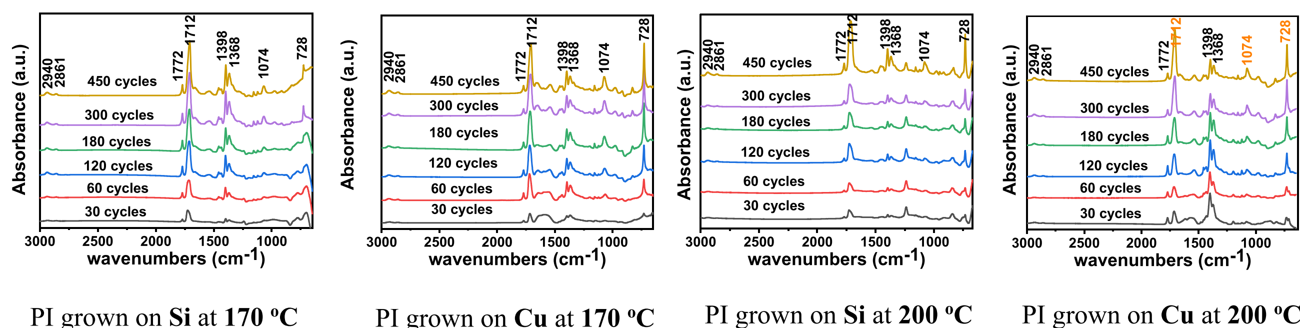

Figure 7. ATR-FTIR absorption spectra of polyimide thin films deposited on native SiO_2 and Cu at 170 and 200 °C with MLD cycle numbers increasing from 30 to 450. In the rightmost graph, the numbers highlighted in orange represent the possible IR peaks coming from the interchain PI while both of the numbers in orange and black represent the characteristic IR peaks from the cyclic PI.

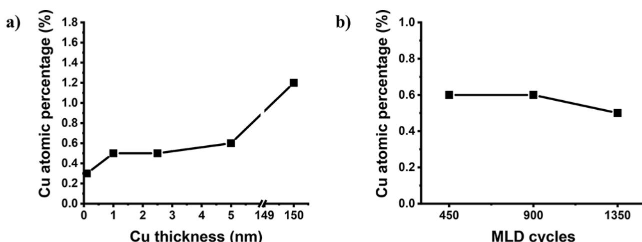

Figure 8. High-resolution XPS was performed on different PI/Cu samples where the PI films were deposited on Cu (a) with the same number of MLD cycle (450 cycles) but with a different Cu thickness from 0.1 to 150 nm and (b) with the same Cu thickness (5 nm) but with a different number of MLD cycles from 450 to 1350.

In these samples, the PI films had a thickness of at least 300 nm, and therefore no copper signal can originate from the Cu layers under the PI films. The detection of about 0.3−1.0 at. % of copper on these PI film surfaces by XPS evidence that copper diffuses through the growing film and presents on the film surfaces (Figure S2 shows a survey scan and a fine scan of XPS spectra of one representative PI sample). It is worth mentioning that copper was present mainly as Cu^{n+} (n = 1, 2) ions. ToF-ERDA measurements were also attempted on these samples, but the PI films eroded so fast during the measurement that it was difficult to determine the existence of copper inside the films. However, if any, concentrations of only 0.02−0.03 at. % Cu were estimated. The existence of Cu ions on the PI film surfaces suggests that small amounts of Cu ions can diffuse inside the deposited PI film, as also reported in other papers.[73−76] The existence of Cu mainly on the film surface indicates that Cu ions somehow float on the film surface and constantly catalyze the formation of the interchain PI. The catalytic efficiency is so high that 1 at. % or less of Cu ions is enough for the catalytic reaction. The high catalytic efficiency was also proved by using the nominally 0.1 nm Cu to promote the MLD growth at 200 °C, as discussed in section 3.1.2.

3.4. Proposed MLD Reaction Mechanism on Cu Surface.

Before we proceed to the discussion on reaction mechanisms in the PI MLD on Cu, it is necessary to clarify that this work focuses on the understanding of reaction mechanisms in the film growth stage, concerning the MLD reaction between the two precursors. Reactions between the precursors and the substrate surface in the nucleation stage are

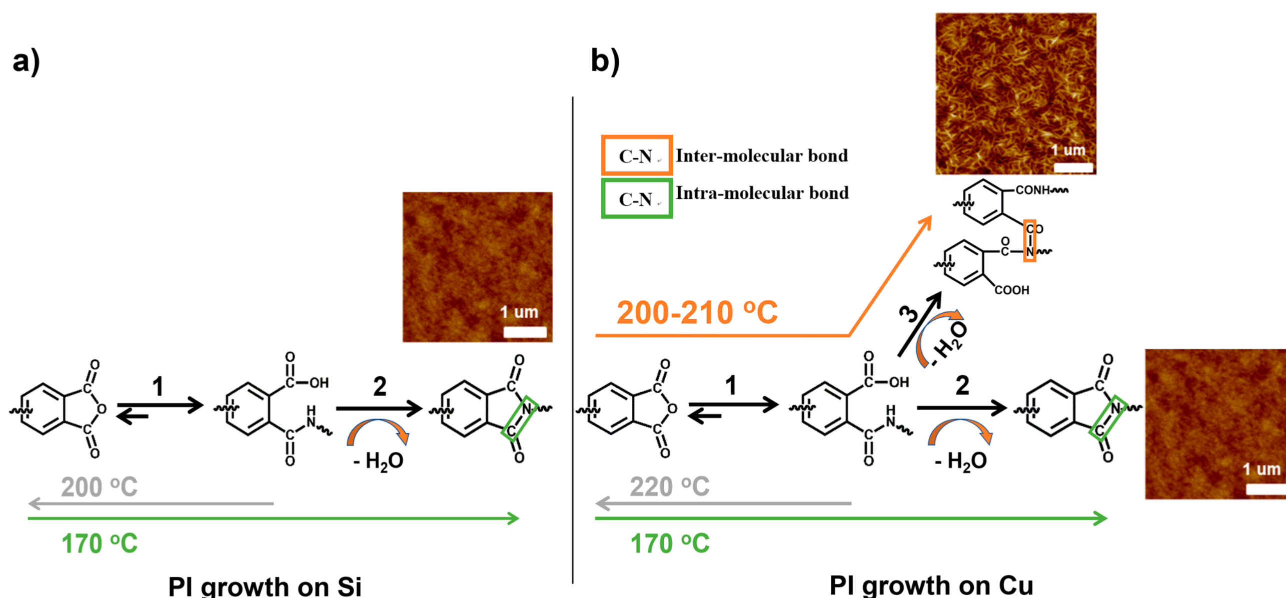

Figure 9. Schematic diagram of the proposed surface reaction between PMDA and DAH leading to (a) the formation of cyclic PI on native SiO_2 and (b) the formation of cyclic PI on Cu at 170 °C and interchain PI at 200−210 °C.

not included since the main cause for the selectivity is suggested to be the new MLD reaction.

Figure 9 shows the proposed reaction mechanisms on Cu and native SiO_2 at different deposition temperatures. The reaction mechanism of imidization to form the ring-closed PI has been well established in previous studies.[61,63−65] We believe that the MLD mechanism in the PI growth on native SiO_2 is the same, as shown in Figure 9a. Imidization is a two-step reaction: first, diamine reacts with its coreactant of dianhydride through reversible amidation (step 1) to form polyamic acid, and the polyamic acid further converts to the ring-closed PI via the irreversible ring-closure reaction (step 2). Generally, after the rapid amidation (step 1) there is a competition between the subsequent ring-closure reaction (step 2) and reversed amidation (reversed step 1), leading to a formation of the ring-closed PI and precursor re-evaporation, respectively. As the deposition temperature increases, the reversed amidation process (reversed step 1) gets faster than the ring-closure reaction (step 2), resulting in a constant decrease in the film growth rate. Although there is some interchain PI forming at 180 °C on native SiO_2, as evidenced by XRD (Figure 5c), the rate of the reaction forming the interchain PI is still much lower than the rate of the precursor desorption. Thereby, the overall growth rate shows a decreasing trend.

For the PI growth on Cu (Figure 9b), the precursors, DAH and PMDA, first react with each other via the same amidation process (step 1) to form the poly(amic acid). This poly(amic acid) as an intermediate species further undergoes two different reaction pathways. One is the ring-closure reaction (step 2), leading to the formation of the ring-closed PI (the C−N bonding for the ring-closure reaction is highlighted by a green box in Figure 9b). The other way is a cross-linking reaction between two adjacent poly(amic acid)s (step 3), leading to the formation of the crystalline interchain PI (the C−N bonding is highlighted by an orange box in Figure 9b). The proceeding of the reactions 2 and 3 is highly dependent on the deposition temperature. At 170 °C there is no evidence of the crystalline interchain PI in the formed films. Thus, it is suggested that amorphous ring-closed PI is predominantly formed on Cu at 170 °C through the ring-closure reaction, the same as on native SiO_2. At 180 °C, a weak diffraction peak was found by XRD (Figure 5b) on a 90 nm thick PI film, indicating the onset of the cross-linking reaction leading to the formation of the interchain PI. As the deposition temperature increases further, the cross-linking reaction gets faster, resulting in an increased film growth rate. At 200−210 °C, the formation of the crystalline interchain PI dominates as evidenced by XRD (Figure 5b) and AFM (Figure 6). Further increasing the temperature to 220 °C causes significant precursor desorption with a sharp decrease in the growth rate also for the interchain PI.

According to our experimental results and the proposed reaction mechanism for the PI MLD on Cu, it appears evident that the selective growth of PI on Cu versus native SiO_2 at 200−210 °C is caused by the preferable formation of the new interchain PI on Cu at these temperatures. Also, as evidenced by XPS results, small amounts of copper ions float on the film surfaces. Hence, the unique growth and structure of PI on copper must be caused by the presence of copper ions which somehow catalyze the formation of the crystalline interchain PI. This conclusion is reached based on the experimental observations, and at this point there is no explanation for how copper ions change the growth mechanism.

4. CONCLUSIONS

In this work, we studied a novel ASD approach in which a high-performance polymer of polyimide was selectively deposited on Cu versus native SiO_2. It was found that the selectivity is highly dependent on the deposition temperature. The optimal selectivity was achieved at deposition temperatures of 200−210 °C where the film growth rate on Cu was about 7.8 Å/cycle while only 0.4 Å/cycle was measured on native SiO_2.

Properties of the PI films deposited on Cu at the selectivity enabling temperature of 200 °C were thoroughly compared with those deposited on Cu and native SiO_2 at the nonselective temperature of 170 °C. According to the results from XRD, AFM, and ATR-FTIR, a novel interchain PI was synthesized and identified. The identification of the new polymer species strongly supports our hypothesis that a different MLD reaction proceeds on Cu at 200−210 °C.

The analysis of reaction mechanisms in PI MLD on native SiO_2 and Cu suggests that the selectivity arises from the preferable formation of interchain PI on Cu through a unique MLD reaction. On the basis of results from XPS, ToF-ERDA, and XRD, it appears that Cu ions catalyze the MLD reaction at 200−210 °C, and small amounts of these Cu ions are sufficient to constantly catalyze the MLD growth by floating on the surface of the growing PI film during the MLD process. The high catalytic efficiency was verified by the successful use of a nominally 0.1 nm Cu seed layer to promote the selective growth. Finally, the severe decrease in the growth rate, caused by the reduction of the oxide layer on the Cu surfaces, further confirmed the importance of copper ions originating from the surface CuO_x (x = 1−2).

■ ASSOCIATED CONTENT

Supporting Information

The Supporting Information is available free of charge at https://pubs.acs.org/doi/10.1021/acs.chemmater.0c00898.

AFM images of PI films deposited on native SiO_2 and Cu surfaces at 170 and 200 °C with different cycle numbers; XPS survey and fine scan spectra for the PI sample that is deposited on a 5 nm thick Cu layer with 1350 MLD cycles at 200 °C, corresponding to the PI thickness around 1000 nm (PDF)

■ AUTHOR INFORMATION

Corresponding Author

Mikko Ritala − *Department of Chemistry, University of Helsinki, 00014 Helsinki, Finland;* orcid.org/0000-0002-6210-2980; Phone: + 358 2941 50193; Email: mikko.ritala@helsinki.fi

Authors

Chao Zhang − *Department of Chemistry, University of Helsinki, 00014 Helsinki, Finland;* orcid.org/0000-0002-9273-2289

Marko Vehkamäki − *Department of Chemistry, University of Helsinki, 00014 Helsinki, Finland*

Mika Pietikäinen − *ASM Microchemistry, 00560 Helsinki, Finland*

Markku Leskelä − *Department of Chemistry, University of Helsinki, 00014 Helsinki, Finland;* orcid.org/0000-0001-5830-2800

Complete contact information is available at:
https://pubs.acs.org/10.1021/acs.chemmater.0c00898

Notes

The authors declare no competing financial interest.

■ ACKNOWLEDGMENTS

Financial support from ASM Microchemistry and China Scholarship Council (File No. 201507040043) is gratefully acknowledged. The authors thank Kenichiro Mizohata for ToF-ERDA measurements and Mikko Heikkila for XRD teaching.

■ REFERENCES

(1) Pan, D. Z.; Liebmann, L.; Yu, B.; Xu, X.; Lin, Y. *Pushing Multiple Patterning in Sub-10 nm: Are We Ready? 52nd ACM/EDAC/IEEE Design Automation Conference (DAC)*; IEEE: San Francisco, CA, June 8−12, 2015.

(2) Mulkens, J.; Hanna, M.; Wei, H.; Vaenkatesan, V.; Megens, H.; Slotboom, D. Overlay and Edge Placement Control Strategies for the 7 nm Node Using EUV and ArF Lithography. Extreme Ultraviolet (EUV) Lithography VI. *Proc. SPIE* **2015**, *9422*, 94221Q.

(3) Clark, R.; Tapily, K.; Yu, K.-H.; Hakamata, T.; Consiglio, S.; O'Meara, D.; Wajda, C.; Smith, J.; Leusink, G. Perspective: New Process Technologies Required for Future Devices and Scaling. *APL Mater.* **2018**, *6*, 058203.

(4) Biyikli, N.; Haider, A.; Deminskyi, P.; Yilmaz, M. Self-Aligned Nanoscale Processing Solutions via Selective Atomic Layer Deposition of Oxide, Nitride, and Metallic Films. *Low-Dimensional Materials and Devices 2017*; SPIE: 2017, *10349*, 103490M.

(5) Leskelä, M.; Ritala, M. Atomic Layer Deposition (ALD): From Precursors to Thin Film Structures. *Thin Solid Films* **2002**, *409*, 138−146.

(6) Mackus, A. J. M.; Bol, A. A.; Kessels, W. M. The Use of Atomic Layer Deposition in Advanced Nanopatterning. *Nanoscale* **2014**, *6*, 10941−10960.

(7) Chen, R.; Bent, S. F. Chemistry for Positive Pattern Transfer Using Area-Selective Atomic Layer Deposition. *Adv. Mater.* **2006**, *18*, 1086−1090.

(8) Chen, R.; Bent, S. F. Highly Stable Monolayer Resists for Atomic Layer Deposition on Germanium and Silicon. *Chem. Mater.* **2006**, *18*, 3733−3741.

(9) Chen, R.; Kim, H.; McIntyre, P. C.; Bent, S. F. Investigation of Self-Assembled Monolayer Resists for Hafnium Dioxide Atomic Layer Deposition. *Chem. Mater.* **2005**, *17*, 536−544.

(10) Bobb-Semple, D.; Nardi, K. L.; Draeger, N.; Hausmann, D. M.; Bent, S. F. Area-Selective Atomic Layer Deposition Assisted by Self-Assembled Monolayers: A Comparison of Cu, Co, W, and Ru. *Chem. Mater.* **2019**, *31*, 1635−1645.

(11) Singh, J. A.; Thissen, N. F. W.; Kim, W.-H.; Johnson, H.; Kessels, W. M. M.; Bol, A. A.; Bent, S. F.; Mackus, A. J. M. Area-Selective Atomic Layer Deposition of Metal Oxides on Noble Metals through Catalytic Oxygen Activation. *Chem. Mater.* **2018**, *30*, 663−670.

(12) Mackus, A. J. M.; Dielissen, S.; Mulders, J.; Kessels, W. M. Nanopatterning by Direct-Write Atomic Layer Deposition. *Nanoscale* **2012**, *4*, 4477−4480.

(13) Mackus, A. J. M.; Thissen, N.; Mulders, J.; Trompenaars, P.; Verheijen, M.; Bol, A. A.; Kessels, W. M. Direct-Write Atomic Layer Deposition of High-Quality Pt Nanostructures: Selective Growth Conditions and Seed Layer Requirements. *J. Phys. Chem. C* **2013**, *117*, 10788−10798.

(14) Färm, E.; Lindroos, S.; Ritala, M.; Leskelä, M. Microcontact Printed RuO_x Film as an Activation Layer for Selective-Area Atomic Layer Deposition of Ruthenium. *Chem. Mater.* **2012**, *24*, 275−278.

(15) Mameli, A.; Karasulu, B.; Verheijen, M. A.; Barcones, B.; Macco, B.; Mackus, A. J. M.; Kessels, W. M.; Roozeboom, F. Area-Selective Atomic Layer Deposition of ZnO by Area Activation Using Electron Beam-Induced Deposition. *Chem. Mater.* **2019**, *31*, 1250−1257.

(16) Atanasov, S. E.; Kalanyan, B.; Parsons, G. N. Inherent Substrate-Dependent Growth Initiation and Selective-Area Atomic Layer Deposition of TiO_2 Using "Water-Free" Metal-Halide/Metal Alkoxide Reactants. *J. Vac. Sci. Technol., A* **2016**, *34*, 01A148.

(17) Mackus, A. J. M.; Merkx, M. J. M.; Kessels, W. M. M. From the Bottom-Up: Toward Area-Selective Atomic Layer Deposition with High Selectivity. *Chem. Mater.* **2019**, *31*, 2−12.

(18) Cao, K.; Cai, J.; Liu, X.; Chen, R. Catalysts Design and Synthesis via Selective Atomic Layer Deposition. *J. Vac. Sci. Technol., A* **2018**, *36*, 010801.

(19) Du, Y.; George, S. M. Molecular Layer Deposition of Nylon 66 Films Examined Using In Situ FTIR Spectroscopy. *J. Phys. Chem. C* **2007**, *111*, 8509−8517.

(20) Putkonen, M.; Harjuoja, J.; Sajavaara, T.; Niinistö, L. Atomic Layer Deposition of Polyimide Thin Films. *J. Mater. Chem.* **2007**, *17*, 664−669.

(21) Miyamae, T.; Tsukagoshi, K.; Matsuoka, O.; Yamamoto, S.; Nozoye, H. Preparation of Polyimide-Polyamide Random Copolymer Thin Film by Sequential Vapor Deposition Polymerization. *Jpn. J. Appl. Phys.* **2002**, *41*, 746−748.

(22) Kim, A.; Filler, M. A.; Kim, S.; Bent, S. F. Layer-by-Layer Growth on Ge (100) via Spontaneous Urea Coupling Reactions. *J. Am. Chem. Soc.* **2005**, *127*, 6123−6132.

(23) Park, Y.-S.; Kim, H.; Cho, B.; Lee, C.; Choi, S.-E.; Sung, M. M.; Lee, J. S. Intramolecular and Intermolecular Interactions in Hybrid Organic−Inorganic Alucone Films Grown by Molecular Layer Deposition. *ACS Appl. Mater. Interfaces* **2016**, *8*, 17489−17498.

(24) Dameron, A. A.; Seghete, D.; Burton, B.; Davidson, S.; Cavanagh, A.; Bertrand, J.; George, S. M. Molecular Layer Deposition of Alucone Polymer Films Using Trimethylaluminum and Ethylene Glycol. *Chem. Mater.* **2008**, *20*, 3315−3326.

(25) George, S. M.; Yoon, B.; Dameron, A. A. Surface Chemistry for Molecular Layer Deposition of Organic and Hybrid Organic-Inorganic Polymers. *Acc. Chem. Res.* **2009**, *42*, 498−508.

(26) Zhou, H.; Bent, S. F. Fabrication of Organic Interfacial Layers by Molecular Layer Deposition: Present Status and Future Opportunities. *J. Vac. Sci. Technol., A* **2013**, *31*, 040801.

(27) Sarkar, D.; Ishchuk, S.; Taffa, D. H.; Kaynan, N.; Berke, B. A.; Bendikov, T.; Yerushalmi, R. Molecular Layer Deposition of Hybrid Organic−Inorganic Thin Films as Precursors for Enhanced Photocatalysis. *J. Phys. Chem. C* **2016**, *120*, 3853−3862.

(28) Piper, D. M.; Travis, J. J.; Young, M.; Son, S.-B.; Kim, S. C.; Oh, K. H.; George, S. M.; Ban, C.; Lee, S.-H. Reversible High-Capacity Si Nanocomposite Anodes for Lithium-Ion Batteries Enabled by Molecular Layer Deposition. *Adv. Mater.* **2014**, *26*, 1596−1601.

(29) Zhao, Y.; Sun, X. Molecular Layer Deposition for Energy Conversion and Storage. *Acs Energy Lett.* **2018**, *3*, 899−914.

(30) Sun, Q.; Lau, K. C.; Geng, D.; Meng, X. Atomic and Molecular Layer Deposition for Superior Lithium-Sulfur Batteries: Strategies, Performance, and Mechanisms. *Batteries & Supercaps.* **2018**, *1*, 41−68.

(31) Lee, K.; Kim, J.; Shin, K.; Kim, Y. S. Micropatterned Crystalline Organic Semiconductors via Direct Pattern Transfer Printing with PDMS Stamp. *J. Mater. Chem.* **2012**, *22*, 22763−22768.

(32) Cavallini, M.; Stoliar, P.; Moulin, J.-F.; Surin, M.; Leclère, P.; Lazzaroni, R.; Breiby, D. W.; Andreasen, J. W.; Nielsen, M. M.; Sonar, P.; Grimsdale, A. C.; Müllen, K.; Biscarini, F. Field-Effect Transistors Based on Self-Organized Molecular Nanostripes. *Nano Lett.* **2005**, *5*, 2422−2425.

(33) Serban, D. A.; Greco, P.; Melinte, S.; Vlad, A.; Dutu, C. A.; Zacchini, S.; Iapalucci, M. C.; Biscarini, F.; Cavallini, M. Towards All-

Organic Field-Effect Transistors by Additive Soft Lithography. *Small* **2009**, *5*, 1117−1122.
(34) Cavallini, M.; D'Angelo, P.; Criado, V. V.; Gentili, D.; Shehu, A.; Leonardi, F.; Milita, S.; Liscio, F.; Biscarini, F. Ambipolar Multi-Stripe Organic Field-Effect Transistors. *Adv. Mater.* **2011**, *23*, 5091−5097.
(35) Prasittichai, C.; Pickrahn, K. L.; Minaye Hashemi, F. S.; Bergsman, D. S.; Bent, S. F. Improving Area-Selective Molecular Layer Deposition by Selective SAM Removal. *ACS Appl. Mater. Interfaces* **2014**, *6*, 17831−17836.
(36) Hashemi, F. S. M.; Prasittichai, C.; Bent, S. F. A New Resist for Area Selective Atomic and Molecular Layer Deposition on Metal−Dielectric Patterns. *J. Phys. Chem. C* **2014**, *118*, 10957−10962.
(37) Prasittichai, C.; Zhou, H.; Bent, S. F. Area Selective Molecular Layer Deposition of Polyurea Films. *ACS Appl. Mater. Interfaces* **2013**, *5*, 13391−13396.
(38) Maier, G. Low Dielectric Constant Polymers for Micro-electronics. *Prog. Polym. Sci.* **2001**, *26*, 3−65.
(39) Yuan, C.; Jin, K.; Li, K.; Diao, S.; Tong, J.; Fang, Q. Non-Porous Low-K Dielectric Films Based on a New Structural Amorphous Fluoropolymer. *Adv. Mater.* **2013**, *25*, 4875−4878.
(40) Muruganand, S.; Narayandass, S. K.; Mangalaraj, D.; Vijayan, T. M. Dielectric and Conduction Properties of Pure Polyimide Films. *Polym. Int.* **2001**, *50*, 1089−1094.
(41) Kato, Y.; Iba, S.; Teramoto, R.; Sekitani, T.; Someya, T.; Kawaguchi, H.; Sakurai, T. High Mobility of Pentacene Field-Effect Transistors with Polyimide Gate Dielectric Layers. *Appl. Phys. Lett.* **2004**, *84*, 3789−3791.
(42) Unni, K. N.; Dabos-Seignon, S.; Nunzi, J.-M. Improved Performance of Pentacene Field-Effect Transistors Using a Polyimide Gate Dielectric Layer. *J. Phys. D: Appl. Phys.* **2005**, *38*, 1148−1151.
(43) Zhen, L.; Guan, W.; Shang, L.; Liu, M.; Liu, G. Organic Thin-Film Transistor Memory with Gold Nanocrystals Embedded in Polyimide Gate Dielectric. *J. Phys. D: Appl. Phys.* **2008**, *41*, 135111.
(44) Yoshimura, T.; Tatsuura, S.; Sotoyama, W. Polymer Films Formed with Monolayer Growth Steps by Molecular Layer Deposition. *Appl. Phys. Lett.* **1991**, *59*, 482−484.
(45) Peng, Q.; Gong, B.; VanGundy, R. M.; Parsons, G. N. Zincone" Zinc Oxide- Organic Hybrid Polymer Thin Films Formed by Molecular Layer Deposition. *Chem. Mater.* **2009**, *21*, 820−830.
(46) Ju, L.; Vemuri, V.; Strandwitz, N. C. Quartz Crystal Microbalance Study of Precursor Diffusion During Molecular Layer Deposition Using Cyclic Azasilane, Maleic Anhydride, and Water. *J. Vac. Sci. Technol., A* **2019**, *37*, 030909.
(47) Stevens, E.; Tomczak, Y.; Chan, B. T.; Altamirano Sanchez, E.; Parsons, G. N.; Delabie, A. Area-Selective Atomic Layer Deposition of TiN, TiO_2, and HfO_2 on Silicon Nitride with Inhibition on Amorphous Carbon. *Chem. Mater.* **2018**, *30*, 3223−3232.
(48) Kalanyan, B.; Lemaire, P. C.; Atanasov, S. E.; Ritz, M. J.; Parsons, G. N. Using Hydrogen to Expand the Inherent Substrate Selectivity Window During Tungsten Atomic Layer Deposition. *Chem. Mater.* **2016**, *28*, 117−126.
(49) Kannan Selvaraj, S.; Parulekar, J.; Takoudis, C. G. Selective Atomic Layer Deposition of Zirconia on Copper Patterned Silicon Substrates Using Ethanol as Oxygen Source as well as Copper Reductant. *J. Vac. Sci. Technol., A* **2014**, *32*, 010601.
(50) Tao, Q.; Jursich, G.; Takoudis, C. Selective Atomic Layer Deposition of HfO_2 on Copper Patterned Silicon Substrates. *Appl. Phys. Lett.* **2010**, *96*, 192105.
(51) Song, S. K.; Saare, H.; Parsons, G. N. Integrated Isothermal Atomic Layer Deposition/Atomic Layer Etching Supercycles for Area-Selective Deposition of TiO_2. *Chem. Mater.* **2019**, *31*, 4793−4804.
(52) Vallat, R.; Gassilloud, R.; Salicio, O.; El Hajjam, K.; Molas, G.; Pelissier, B.; Vallée, C. Area Selective Deposition of TiO_2 by Intercalation of Plasma Etching Cycles in PEALD Process: A Bottom Up Approach for the Simplification of 3D Integration Scheme. *J. Vac. Sci. Technol., A* **2019**, *37*, 020918.
(53) Vos, M. F. J.; Chopra, S. N.; Verheijen, M. A.; Ekerdt, J. G.; Agarwal, S.; Kessels, W. M. M.; Mackus, A. J. M. Area-Selective Deposition of Ruthenium by Combining Atomic Layer Deposition and Selective Etching. *Chem. Mater.* **2019**, *31*, 3878−3882.
(54) Vallat, R.; Gassilloud, R.; Eychenne, B.; Vallée, C. Selective Deposition of Ta_2O_5 by Adding Plasma Etching Super-Cycles in Plasma Enhanced Atomic Layer Deposition Steps. *J. Vac. Sci. Technol., A* **2017**, *35*, 01B104.
(55) Soininen, P.; Elers, K.-E.; Saanila, V.; Kaipio, S.; Sajavaara, T.; Haukka, S. Reduction of Copper Oxide Film to Elemental Copper. *J. Electrochem. Soc.* **2005**, *152*, G122−G125.
(56) Yang, W.; Shintani, H.; Akaike, M.; Suga, T. Low Temperature Cu-Cu Direct Bonding Using Formic Acid Vapor Pretreatment. *Electronic Components and Technology Conference (ECTC)*; IEEE: 61st, 2011.
(57) Singh, B.; Hyun, J. Y.; Singh, A. P.; Gandhi, D.; Wu, Z.; Interrante, L. V.; Ramanath, G. Selective Deposition of a Cross-Linked Low-Permittivity Polycarbosilane on Copper. *ACS Appl. Mater. Interfaces* **2010**, *2*, 2180−2184.
(58) Sheng, T.; Chen, H.; Xiong, S.; Chen, X.; Wang, Y. Atomic Layer Deposition of Polyimide on Microporous Polyethersulfone Membranes for Enhanced and Tunable Performances. *AIChE J.* **2014**, *60*, 3614−3622.
(59) Spassova, E. Vacuum Deposited Polyimide Thin Films. *Vacuum* **2003**, *70*, 551−561.
(60) Tsai, F. Y.; Alfonso, E. L.; Harding, D. R.; Chen, S. H. Processing Vapour-Deposited Polyimide. *J. Phys. D: Appl. Phys.* **2001**, *34*, 3011.
(61) Bitzer, T.; Richardson, N. V. Demonstration of an Imide Coupling Reaction on a Si(100)-2 × 1 Surface by Molecular Layer Deposition. *Appl. Phys. Lett.* **1997**, *71*, 662−664.
(62) Koning, C.; Teuwen, L.; Meijer, E.W.; Moonen, J. Synthesis and Properties of α, ø-Diaminoalkane Based Polyimides. *Polymer* **1994**, *35*, 4889−4895.
(63) Sacher, E. A Reexamination of Polyimide Formation. *J. Macromol. Sci., Part B: Phys.* **1986**, *25*, 405−418.
(64) Snyder, R.; Thomson, B.; Bartges, B.; Czerniawski, D.; Painter, P. FTIR Studies of Polyimides: Thermal Curing. *Macromolecules* **1989**, *22*, 4166−4172.
(65) Jou, J. H.; Huang, P. T. Effect of Thermal Curing on the Structures and Properties of Aromatic Polyimide Films. *Macromolecules* **1991**, *24*, 3796−3803.
(66) Gan, S.; Seferis, J. C. Heated Stage IR Microscopy for Cure Studies of Polyimide Matrix Composites. *Sci. Eng. Compos. Mater.* **1992**, *2*, 119−128.
(67) Jou, J.-H.; Huang, P.-T. X-Ray Diffraction Study of Polyimide Blends Compatibility. *Polym. J.* **1990**, *22*, 909−918.
(68) Cotts, P. M.; Volksen, W. Solution Characterization of Polyamic Acids and Polyimides. *ACS Symp. Ser.* **1984**, *242*, 227−237.
(69) Russell, T. A Small-Angle X-Ray Scattering Study of an Aromatic Polyimide. *J. Polym. Sci., Polym. Phys. Ed.* **1984**, *22*, 1105−1117.
(70) Russell, T.; Gugger, H.; Swalen, J. In-Plane Orientation of Polyimide. *J. Polym. Sci., Polym. Phys. Ed.* **1983**, *21*, 1745−1756.
(71) Isoda, S.; Shimada, H.; Kochi, M.; Kambe, H. Molecular Aggregation of Solid Aromatic Polymers. I. Small-Angle X-Ray Scattering from Aromatic Polyimide Film. *J. Polym. Sci., Polym. Phys. Ed.* **1981**, *19*, 1293−1312.
(72) Pryde, C. A. IR Studies of Polyimides. I. Effects of Chemical and Physical Changes During Cure. *J. Polym. Sci., Part A: Polym. Chem.* **1989**, *27*, 711−724.
(73) Faupel, F.; Gupta, D.; Silverman, B. D.; Ho, P. S. Direct Measurements of Cu Diffusion into a Polyimide Below the Glass Transition Temperature. *Appl. Phys. Lett.* **1989**, *55*, 357−359.
(74) Faupel, F.; Willecke, R.; Thran, A. Diffusion of Metals in Polymers. *Mater. Sci. Eng., R* **1998**, *22*, 1−55.
(75) Kim, N. Y.; Yoon, H. S.; Kim, S. Y.; Whang, C. N.; Kim, K. W.; Cho, S. J. Diffusion of Copper into Polyimide Deposited by Ionized Cluster Beam. *J. Vac. Sci. Technol., B: Microelectron. Process. Phenom.* **1999**, *17*, 380−384.

(76) Liang, T.; Liu, Y.; Fu, Z.; Luo, T.; Zhang, K. Diffusion and Adhesion Properties of Cu Films on Polyimide Substrates. *Thin Solid Films* **2005**, *473*, 247−251.

https://dx.doi.org/10.1021/acs.chemmater.0c00898
Chem. Mater. 2020, 32, 5073−5083